# Single plasmonic split hole resonator nanostructure as an efficient nanoscale light source

P.N. Melentiev, A.E. Afanasiev, V.I. Balykin

***Abstract.*** **We report a brief review of the results of experimental studies on the nonlinear optical interaction of laser radiation with a hybrid plasmonic nanostructure, i.e. a split hole resonator (SHR). We demonstrate second- and third-harmonic generation and mixed-frequency generation from a single SHR nanostructure. The practical application potential of an SHR nanostructure as a nanoprobe for measuring the femtosecond laser pulse duration and designing an all-optical nanodisplay is shown.**

## 1. Introduction

Interest in single plasmonic nanostructures is caused in many respects by the possibility of using them in schemes of all-optical data control and information transfer [1], in which plasmonic nanostructures make it possible not only to detect radiation with a nanoscale spatial accuracy and subfemtosecond temporal resolution but also to control it [2]. However, recent studies have shown that the application potential of single plasmonic nanostructures is much greater and includes the study of the optical properties of metals at a nanoscale level, investigation of the structures of their electron levels (including quantum effects), analysis of various types of optical nonlinear interactions, design of highly sensitive sensors, analysis of temporal properties of pulsed laser radiation, design of optical tweezers, etc. [3].

It is well known that the frequencies of localised-plasmon resonances can be determined by the size, shape, and material composition of the nanoparticle [4–6]. One should consider separately two cases, where the nanostructure size is either smaller or larger than the metal skin depth. In the former case, the optical interaction of light with a nanoparticle can be described in terms of the so-called quasi-static approach, where the plasmon resonance frequencies are determined by the optical constants of the material of nanostructures and are independent of their size [7]. In the latter case, the plasmon resonances depend strongly on the size

**P.N. Melentiev, A.E. Afanasiev, V.I. Balykin** Institute for Spectroscopy, Russian Academy of Sciences, ul. Fizicheskaya 5, Troitsk, 108840 Moscow region, Russia; e-mail: melentiev@isan.troitsk.ru, afanasiev.isan@gmail.com, balykin@isan.troitsk.ru

and geometry of nanostructures, and their spectral position is adequately described within the Mie theory [7]. Under these conditions, according to the Mie theory it is convenient to analyse the optical interaction with nanostructures by expanding the polarisation induced in a nanostructure in multipoles. In this expansion, excited localised plasmon resonances of different orders, corresponding to the multipole excitation, can be selected in the nanoparticle optical response [8–11].

A solution of the Laplace equation with the corresponding boundary conditions shows that an effective multipolar polarisability may arise in a sphere of radius $R$, characterised by a permittivity $\tilde{\varepsilon}_{\mathrm{p}}(\omega)$ and located in a medium with a permittivity $\varepsilon_{\mathrm{out}}$ [12]:

$$\tilde{\alpha}_l(\omega) = R^{2l+1}[\tilde{\varepsilon}_{\mathrm{p}}(\omega) - \varepsilon_{\mathrm{out}}]\left[\tilde{\varepsilon}_{\mathrm{p}}(\omega) + \frac{l+1}{l}\varepsilon_{\mathrm{out}}\right]^{-1}, \qquad (1)$$

where the parameter $l$ determines the multipolarity order ($l = 1$ for the dipole resonance, $l = 2$ for the quadrupole resonance, etc.). The contribution of the quadrupole term to the optical response of a nanoparticle becomes significant even when its size reaches $\sim$30 nm, which corresponds to the characteristic values of the skin-layer thickness in the visible spectral range. The quadrupole resonance in the Drude model arises at the frequency

$$\omega_{\mathrm{LSP}} = \frac{\omega_{\mathrm{p}}}{\sqrt{1 + {}^3\!/_2\,\varepsilon_{\mathrm{out}}}} \qquad (2)$$

($\omega_{\mathrm{p}}$ is the plasma frequency of the nanoparticle metal), i.e., at an energy exceeding the dipole-resonance energy. The spectral response of the nanoparticle is still determined by the dipole resonance, but the contributions of multipole resonances increase with increasing nanoparticle size. For high-order resonances, the resonance condition approaches that for surface plasmon polaritons: $\varepsilon_{\mathrm{p}}(\omega) = -\varepsilon_{\mathrm{out}}$. In addition, the radiation scattering from the nanoparticle begins to play an important role. It becomes pronounced at a nanoparticle radius of $\sim$20 nm and dominates in extinction at radii above 100 nm.

We considered the interaction of laser light with a single plasmonic nanostructure having a specially developed geometry [a split hole resonator (SHR)], the variety of optical phenomena accompanying this interaction, and the possibility of their practical application in the design of optical nanodevices. The interactions of an SHR nanostructure with low- and high-intensity light fields (linear and nonlinear optical interactions, respectively) are analysed.

## 2. Nanoparticle and a nano-opening complementary to it: the Babinet principle

The Babinet principle [13, 14] is a classical concept of the wave theory of light. In the scalar formulation, the Babinet principle establishes a correspondence between the diffraction field on some screen and the field on the so-called additional screen. In a more rigorous formulation, the Babinet principle suggests that magnetic and electric fields are interchangeable with respect to an ideally conducting planar structured screen and a complementary screen [14]. The Babinet principle makes it possible to solve some problems of classical electrodynamics related to electromagnetic wave scattering by passing to another (equivalent) problem, the solution to which is either known or can be found more easily.

In accordance with the Babinet principle, a metal nanoparticle (disk) and a nanohole complementary to it have complementary optical spectra when these structures are exposed to light with the corresponding (mutually orthogonal) polarisations: the maximum transmission in the hole is observed when light is quenched in the complementary particle.

Note that the Babinet principle was formulated and proven for the structures formed by an ideal conductor with infinite conductivity. However, as modern studies have shown, this principle can also be applied to metals with a finite conductivity. In this case, one cannot speak about completely complementary interaction of light with Babinet-complementary structures based on real metals. However, the Babinet principle makes it possible to find some regularities in the solution of these problems, which is especially important when designing the geometry of nanostructures with specified optical properties, because one cannot exactly solve the problem of optical interaction with a nanostructure of arbitrary geometry.

In the last decade, many various metal nanostructures have been experimentally and theoretically studied. These are single metal nanoparticles, their arrays [15, 16], and metal nanostructured films [17, 18]. They are considered as building blocks of more complex structures in nanooptics and nanophotonics [19, 20]. The possibility of using the Babinet principle to develop and investigate new designs of metal nanoparticles or thin metal nanostructured films seems attractive. For example, the Babinet principle is often used to design metamaterials and nanoantennas in different spectral ranges: from visible to microwave [21–24].

However, there are fundamental physical limitations on the applicability of the Babinet principle in the optical range. The boundary conditions for a metal nanostructure are not strictly applicable, because in this case the field penetration depth is comparable with the structure size. In addition, nanostructures are characterised by relatively high losses in the optical range. A question arises: to what extent is the Babinet principle applicable to metal nanostructures in the optical range?

The use of the Babinet principle to predict the response of metal plasmonic nanostructures with sizes much smaller than optical wavelengths does not always lead to conclusions consistent with experimental data, which is due to the finite skin-depth value in most cases. The situation appears to be even more difficult when the nonlinear properties of metal nanostructures are considered [25–28].

Let us consider, as an example, how the Babinet principle can be used to describe the light transmission through a nanohole. In particular, it follows from the Babinet principle that a nanohole in a conducting screen and a nanoparticle (nanodisk) can be characterised by equivalent induced electric and/or magnetic moments. Indeed, as was shown in [29], the field at a large distance from the hole is equivalent to the field induced by two dipoles: a magnetic dipole oriented parallel to the screen and an electric dipole oriented perpendicular to the screen. Rigorous numerical calculations [30, 31] confirmed the main conclusions about the optical response of a nanohole and showed also that the corresponding scattering cross section is smaller than the geometric cross section at a hole radius $a < 0.2\lambda$. Localised plasmon resonances may arise in real metal screens, which affect the transmission cross section [32, 33].

Despite the aforementioned problems related to the use of the Babinet principle, it is nevertheless a valuable landmark in designing metal nanostructures. At the same time, one must take into account its application limits.

## 3. Heat on the nanoscale: nanoparticle and nanohole

When studying the interaction of laser radiation with nanostructures, it is important to remember that resonance metal nanostructures are strong light absorbers. In particular, light incident on a nanostructure may almost entirely be converted into heat [34–38]. The scattering cross section of a metal nanostructure also increases at the resonance frequency. The absorption cross section at the resonance frequency is on the order of the squared radiation wavelength and may exceed several times the physical cross section of the nanostructure. Depending on the size of the nanostructure, scattering or absorption dominates. For small sizes (less than 15 nm), absorption over scattering is dominant, and vice versa.

The physics of heat transfer is quite different on macro- and micro-spatial scales. Heat transfer on the macroscale is considered to be a slow process (in particular, the heat-conduction characteristic time in macroscopic systems about 1 m in size is several minutes). At the same time, the heat propagation at the microscopic level is an extremely fast and efficient process with a characteristic time of $\sim 10$ ns. The microscale heat transfer is practically inertialess. This statement is even more true when the heat transfer on the nanoscale is considered. The reason is the difference in the heat transfer mechanisms: it is a combination of phonon and electron transports at the macroscopic level and a radiative transport at the microscopic level.

Important characteristics of the absorption of laser radiation by a nanoparticle are its temperature and the temporal and spatial dependences of the nanoparticle and environment. These parameters depend strongly on the illumination regime (continuous or pulsed). Heat release occurs after the illumination because of the fast dephasing of coherent electron motion in combination with the fast energy transfer to the metal lattice [39–41]. Heat generation occurs very rapidly, and the thermalisation time is on the order of few picoseconds. On the other hand, the ambient temperature increases for a much longer time (determined by the physical mechanisms of thermal conductivity).

It was shown in [42] that the geometry and environment of a nanostructure affect significantly its heating under pulsed laser irradiation. For example, as compared with a Babinet-complementary structure fabricated in a metal film, a metal nanostructure undergoes thermal destruction at a lower laser beam intensity (Fig. 1). Figure 1a shows a calculated temperature distribution in an aluminum nanorod $50\times570$ nm in
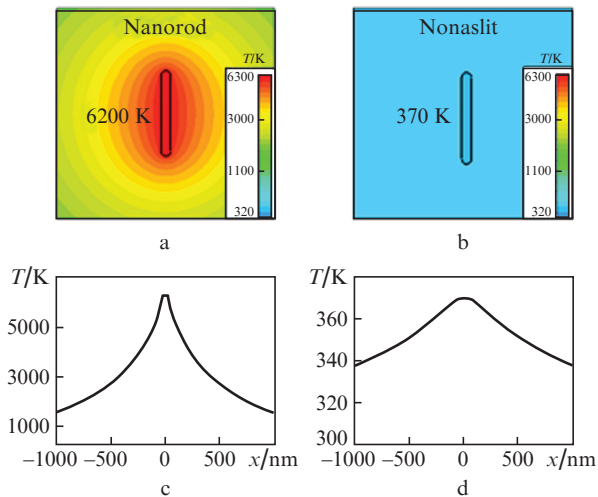
**Figure 1.** (Colour online) (a, b) Calculated 2D spatial temperature distributions and (c, d) their one-dimensional cuts for two complementary nanostructures (nanorod and nanoslit) upon laser heating: (a, c) an aluminium nanorod $50 \times 50 \times 570$ nm in size and (b, d) a $50 \times 570$ nm nanoslit made in 50-nm-thick aluminium film.

size, and Fig. 1b presents a similar distribution for a nanoslit of the same size, fabricated in a 50-nm-thick aluminium film. Both structures are illuminated by a plane monochromatic wave with $\lambda = 1560$ nm; the radiation intensity is $8 \times 10^{13}$ W cm$^{-2}$. The light beam for the nanorod is polarised along its axis, while in the case of the nanoslit it is polarised perpendicular to the large nanorod size. Thus, resonance excitation of plasmonic oscillations is implemented in both cases. It can be seen in Fig. 1 that, at the same radiation intensity, the nanorod is heated to much higher (by more than an order of magnitude) temperatures than the nanoslit.

## 4. Hybrid plasmonic SHR nanostructure

A new concept of a nanostructure, combining the advantages of a nanorod-type structure (strong nonlinear properties) and a nanohole in a metal screen (the absence of background illumination and stability to high radiation intensity) was proposed in [43] based on the Babinet principle and the thermal behaviour of nanostructures in a strong laser field. This nanostructure is a combination of a nanohole fabricated in a metal film and a nanorod located in this nanohole (Fig. 2); it was referred to as a split hole resonator (SHR) [43]. In a certain sense, it is complementary to the known split ring resonator (SRR) nanostructure [25–28, 44].

Calculations showed that the radiation conversion efficiency in an SHR nanostructure depends strongly on its geometry (nanostructure diameter and nanorod length), the film material, and the refractive index of the environment. This is explained by the strong dependence of the excitation efficiency of localised plasmonic oscillations on the geometry of the nanostructure and its local environment [45], which determine also the electromagnetic field distribution and amplitude near the nanostructure.

Figure 2b shows a calculated field distribution in an SHR nanostructure illuminated by a plane light wave at $\lambda = 1.56$ μm, corresponding to the plasmon resonance in the nanostructure. It can be seen that this nanostructure forms a single-pole antenna with a field localised near the tip of its nanorod. Calculations [43] showed that the maximum field amplitude
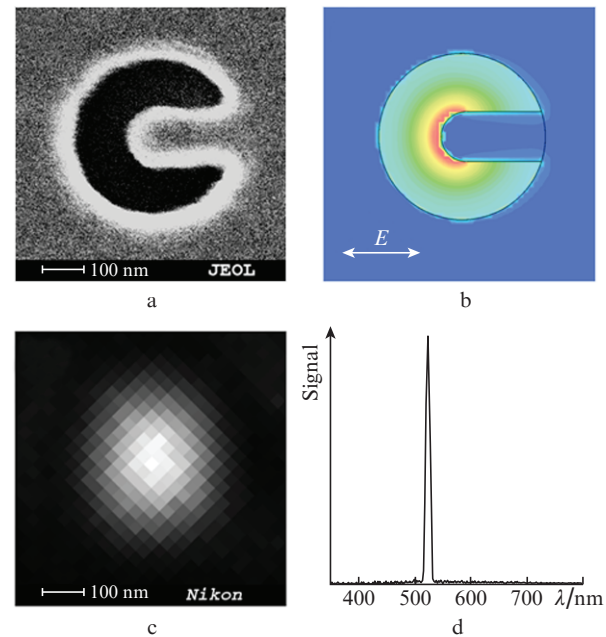


**Figure 2.** (Colour online) (a) Electron microscopy image of an SHR nanostructure fabricated in a 50-nm-thick aluminium film; (b) calculated field distribution for the nanostructure irradiated by a plane monochromatic wave at a wavelength of 1560 nm; (c) optical image of the nanostructure irradiated by 1560-nm laser radiation, with detection at the third-harmonic wavelength (520 nm); and (d) measured third-harmonic spectrum.

in the SHR nanostructure is an order of magnitude larger than for the nanorod at the chosen excitation frequency.

An important property of the SHR nanostructure is the strong dependence of the resonance frequencies of its plasmonic oscillations (and, as a consequence, optical properties) on the nanostructure size and shape. To design a nanostructure with specified optical properties, one must generally control its geometry with an accuracy of the order of $\sim \lambda/10$. In the case of nonlinear processes, the accuracy of the nanostructure geometry should be even higher ($\sim \lambda/100$) [43] in order to control the surface electron states set by sub-nanometre size features on the nanostructure surface.

Controlling the shape and size of nanostructures, one can govern the character of their nonlinear optical interaction with laser radiation (type of nonlinear processes and their efficiency) [43, 46]. For example, the interaction of laser radiation with nanostructures having a 'smooth' surface is mainly characterised by the coherent dynamics of an ensemble of free electrons (plasmons). The result of this interaction is the generation of radiation harmonics. A radically different scenario is implemented for a nanostructure whose surface contains irregularities with a characteristic size of $\sim 10$ nm. In this case, one might expect dominance of the processes related to the dynamics of screened electrons and occurrence of nonlinear optical interaction, which manifests itself as multiphoton luminescence.

### 4.1. Generation of the third harmonic by SHR

Nonlinear optics of metals is in essence the optics of surfaces, nanostructured surfaces, and nanostructures, because radiation penetrates into a metal only at a small depth (on the order of skin depth). Note that the skin depth in the optical range is 30–50 nm, a value comparable with the nanoparticle

size. From the physical point of view, the occurrence of optical nonlinearity in metal nanostructures is due to the electron motion in laser-induced fields [47]. The motion of free electrons of plasmonic nanostructures in strong laser fields is characterised by large oscillation amplitudes. This leads to the manifestation of anharmonicity in the electron cloud motion and, as a consequence, to the occurrence of an effective nonlinear dipole moment [48].

A well-known effect of nonlinear optical interaction of laser radiation with nanostructures is the generation of harmonics [49–56]. To date, numerous studies devoted to the third-harmonic generation from various nanostructures have been performed in nanoplasmonics. The objects of study were metal surfaces [57–63], metal nanostructured surfaces [58, 61, 64–66], nanoparticle ensembles [27, 46, 67–70], and single nanostructures [11, 43, 52, 71–73]. Investigations of metal nanostructures in the form of nanorods (nanoantennas) [71, 72, 74] and nanoholes [11, 68, 75] were performed. The efficiency of nonlinear processes was found to depend strongly on the shape and size of nanostructures. For example, the efficiency for a round nanohole turned out to be several orders of magnitude lower than that for a nanostructure in the form of a nanorod [72] or a nanoslit [42, 75]. This is due to the large difference in the field amplification near nanostructures.

The optical response of an SHR nanostructure depends on its size [43]; a careful choice of the latter should make it possible to implement an efficient third-harmonic generation in the SHR. The most widespread plasmonic material is gold. However, recent studies showed that aluminium has a much higher optical nonlinearity. For example, at a wavelength of 1560 nm, the third-order susceptibility for aluminium is three orders of magnitude higher than that for gold [42, 75]. At a wavelength of 780 nm, this difference reaches about $10^2$ [76]. Thus, an aluminium nanostructure may be a more efficient (in comparison with gold nanoparticles) third-harmonic source. However, at a wavelength of 780 nm, a gold nanostructure exhibits a larger amplification of the field amplitude in comparison with an aluminium nanostructure, which is characterised by very high losses at this wavelength. The reason is that gold has better plasmonic properties at $\lambda = 780$ nm as compared with aluminium (stronger amplification of the local field and lower loss) [42, 75].

The generation of harmonics from nanoparticles at UV frequencies is also of practical interest. First, a solution of this problem will make it possible to implement nanolocalised UV radiation sources, which are necessary for nanodiagnostics and nanolithography. Second, the high optical nonlinearity of nanoparticles in the UV spectral range can be used in cell phototherapy [77]. The generation of UV radiation by plasmonic nanostructures has been poorly studied. There are only few experimental studies [68, 78, 79] where the third-harmonic generation in nanostructures excited by femtosecond laser radiation was demonstrated. For example, a UV-photon flux with an intensity of $10^4$ photons $s^{-1}$ from a single gold nanostructure was obtained in [79].

As was shown in [43], plasmonic resonance modes arise in an SHR nanostructure at some ratio of the hole diameter to the nanorod length (these parameters determine the occurrence of different multipolarities in the nanostructure response). The number of excited modes is controlled by the spectral width of exciting radiation. In the case of a small nanostructure, the number of excited modes is determined by only the nanostructure size and is small. On the contrary, when the nanostructure is large, the number of excited plasmonic modes may be significant, and laser radiation with a rather wide spectrum is necessary for their efficient excitation [11].

The third-harmonic generation in an SHR nanostructure (the geometry of Fig. 2a) was experimentally investigated in [43]. Nanostructures were fabricated by a focused ion beam in a metal film and irradiated by the pulsed femtosecond laser light focused into a small spot. The main features of harmonic generation in an SHR nanostructure is illustrated in Fig. 3. The laser light excites four plasmonic modes in it: dipole mode $\omega_1$ ($\lambda_1 = 750$ nm), multipole ($n = 3$) mode $\omega_2$ ($\lambda_2 = 770$ nm), multipole ($n = 4$) mode $\omega_3$ ($\lambda_3 = 800$ nm), and multipole ($n = 5$) mode $\omega_4$ ($\lambda_4 = 880$ nm). The spectral dependences of the field intensity in these modes are presented in Fig. 3a. To excite the aforementioned localised plasmon resonances, the SHR nanostructure was irradiated by a femtosecond laser pulse (pulse duration of two light-wave cycles), which was focused into a spot several micrometres in diameter [11]. The large spectral width of this laser radiation makes it possible to excite simultaneously four multipole plasmonic modes in the SHR nanostructure.
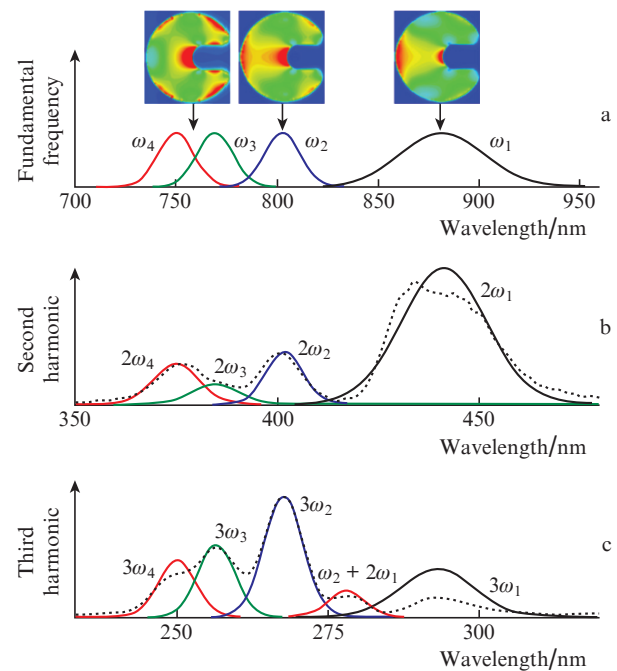


**Figure 3.** (Colour online) Generation of harmonics in an SHR nanostructure: (a) normalised calculated spectral dependences of field intensities for the $\omega_1$, $\omega_2$, $\omega_3$, and $\omega_4$ plasmonic modes and the corresponding calculated distributions of the near-field amplitude in the SHR nanostructure; (b) measured emission spectrum at the second-harmonic frequency (dotted line) and calculated second-harmonic generation spectra corresponding to the excitation of the $\omega_1$, $\omega_2$, $\omega_3$, and $\omega_4$ plasmonic modes in the SHR; and (c) measured emission spectrum at the third-harmonic frequency and calculated third-harmonic generation spectra, corresponding to the excitation of the $\omega_1$, $\omega_2$, $\omega_3$, and $\omega_4$ plasmonic modes in the SHR.

The results of FDTD numerical simulation of the near-field amplitude distribution for an SHR nanostructure irradiated by a monochromatically depolarised laser light beam are presented in Fig. 3a (insets). The simulated near-field amplitude distributions confirm the multipole character of excited

resonances. Due to the spectral proximity of the $\omega_3$ and $\omega_4$ modes, the near field at wavelengths in the vicinity of these resonances is the sum of the near fields of the $\omega_3$ and $\omega_4$ modes.

The excitation of plasmonic modes leads to an increase in the local field at the corresponding wavelengths ($\lambda_1$, $\lambda_2$, $\lambda_3$, $\lambda_4$); therefore, the generation of the second and third harmonics is realised at the double and triple frequencies of these resonances. Figure 3b presents the calculated and measured second-harmonic generation spectra, corresponding to the excitation of the $\omega_1$, $\omega_2$, $\omega_3$, and $\omega_4$ plasmonic modes in the SHR nanostructure. Figure 3c shows the calculated and measured spectra at the third-harmonic frequency, corresponding to the excitation of the $\omega_1$, $\omega_2$, $\omega_3$, and $\omega_4$ plasmonic modes. As was shown in [11], the cross sections of the second- and third-harmonic generation in an SHR nanostructure are, respectively, $\sigma_{\omega \to 2\omega} = 2.4 \times 10^{-18}$ cm$^2$ and $\sigma_{\omega \to 3\omega} = 7 \times 10^{-16}$ cm$^2$. The peak power was found to be $I_{3\omega\,\text{peak}} = 3.4 \times 10^7$ W cm$^{-2}$, and the field amplitude at the third-harmonic frequency reached a significant part of the field amplitude at the fundamental frequency: $E_{3\omega} = 0.006 E_\omega$. Thus, the SHR nanostructure is a UV radiation nanosource of unprecedentedly high intensity and light conversion efficiency, with a UV photon flux of $4 \times 10^8$ photons s$^{-1}$ [11].

### 4.2. Multiphoton luminescence from the SHR

Examples of the manifestation of screened-electron dynamics in plasmonic nanostructures are single-photon [80–82] and multiphoton [83–86] photoluminescence processes. The nonlinear photoluminescence of nanoparticles has actively been investigated in view of numerous applications in spectroscopy and sensing. Among the nonlinear photoluminescence processes, the most thoroughly studied one is the two-photon photoluminescence (2PPL) of gold nanoparticles. A schematic of 2PPL from gold excited by 780-nm radiation [87] is shown in Fig. 4a. The first photon excites an electron via an intraband transition of the sp conduction band. The second photon excites an electron from the d band, and the electron recombines with the sp hole in the conduction band. Photoluminescence arises as a result of the two-photon process of hole generation in the d band and its subsequent recombination with an electron in the sp band. Due to the enhanced density of states, the interband radiative recombination in the case of 2PPL, as well as for conventional PL, occurs near the L and X points of the reciprocal space, as a result of which two emission bands arise (in the green and red spectral ranges, respectively) [87].

The multiphoton photoluminescence is known to be most efficient in small nanostructures [86, 88], a case where localised surface electronic states of screened electrons are formed. An example of manifestation of these surface states is presented in Fig. 5, which shows the results of measuring the emission from a single SHR nanostructure with a nanorod tip containing intentionally fabricated irregularities 5–15 nm in size (Fig. 5a). The other geometric sizes are exactly the same as for the SHR nanostructure shown in Fig. 2. The nanostructure considered in Fig. 5 was irradiated by 1560-nm radiation with the same parameters as for the nanostructure in Fig. 2. Calculations show that the near-field distribution in this nanostructure at the excitation frequency does not differ from the near-field distribution in the nanostructure with a 'smooth' nanorod (see Fig. 2): the spatial field distribution at the fundamental frequency contains
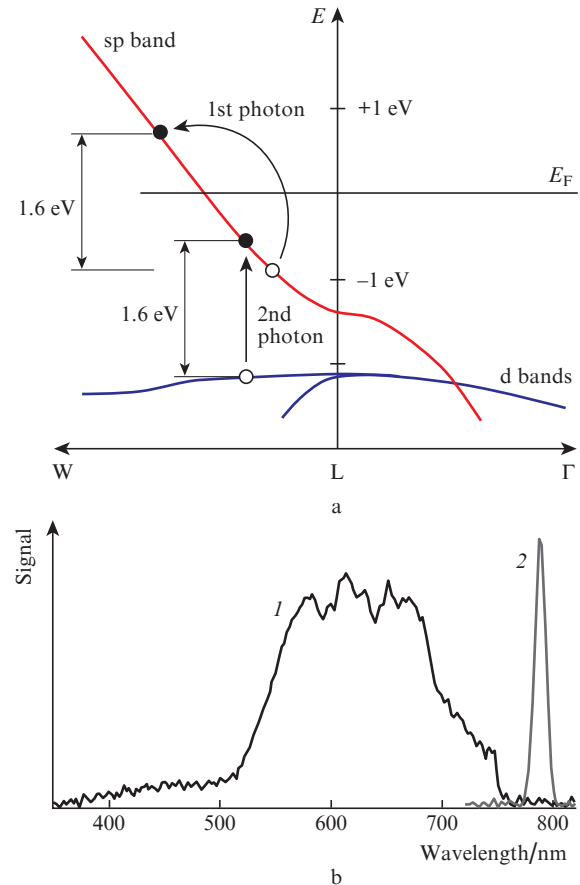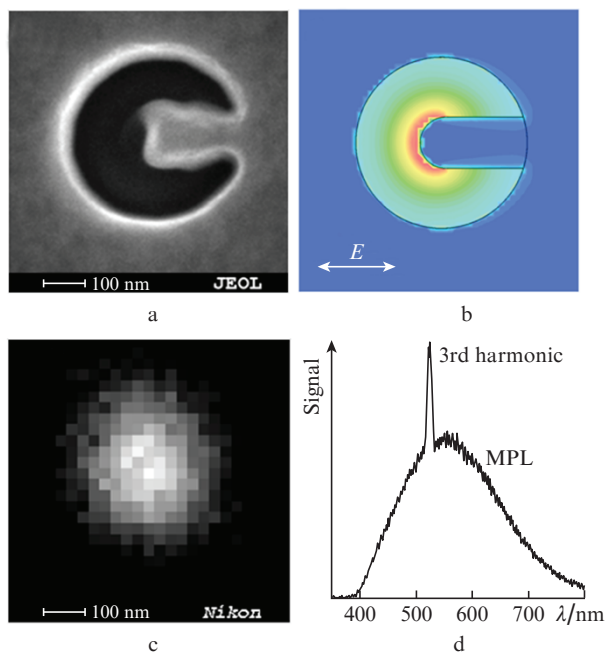


**Figure 4.** (Colour online) Two-photon luminescence in gold: (a) schematic of the gold band structure near the symmetry point L of the first Brillouin zone (multiphoton excitation transfers an electron from the d band to the sp band and (b) measured 2PPL spectrum (*1*) and laser excitation spectrum (*2*).

a pronounced maximum at the nanostructure centre (near the nanorod tip) (Fig. 3b). The optical microscopy image of the nanostructure, recorded in the spectral range of 400–800 nm, contains a spot, whose diameter is limited by the objective numerical aperture (diffraction-limited spot) (Fig. 3c). The emission spectrum of the nanostructure contains, along with a narrow peak due to the third-harmonic generation, a broad band in the range from 390 to more than 800 nm (Fig. 5d). This broad emission band is the result of multiphoton luminescence with an order up to fourth; measurements showed that the dependence of its power on the excitation radiation intensity obeys the power law with an exponent of 3.3. The multiphoton luminescence is the result of excitation of the surface electron states (localised on the aluminium surface) induced on the nanosized inhomogeneities of the aluminium film surface. In the SHR nanostructure, these nanosized inhomogeneities were induced by an ion beam on the nanorod tip (at the point of maximum field at the fundamental frequency).

The photoluminescence efficiency can be significantly increased. It was shown in [86] that photoluminescence can be enhanced by a factor of $10^6$ using a gold nanostructure located near a photonic crystal, which maintains the optical Tamm state at the photoluminescence excitation wavelength.

A possible practical application of 2PPL is the design of nanolocalised broadband laser radiation sources [87].

**Figure 5.** (Colour online) Multiphoton photoluminescence (MPL) from an SHR nanostructure fabricated in a 50-nm-thick aluminium film: (a) electron microscopy image of the nanostructure; (b) calculated field distribution in the nanostructure irradiated by a plane monochromatic wave with $\lambda = 1560$ nm; (c) optical image of the nanostructure illuminated by a laser with $\lambda = 1560$ nm, recorded in the spectral range of $400-800$ nm; and (d) measured MPL spectrum of the nanostructure illuminated by a laser with $\lambda = 1560$ nm.

## 5. SHR-based nanodevices

### 5.1. All-optical nanodisplay

The SHR geometry has a pronounced anisotropy, which is determined by the nanorod direction (see Fig. 2). This fact suggests a polarisation dependence of the SHR optical response to an external laser field. This dependence was investigated by us in [89]. Theoretical calculations of the near-field distribution in an SHR nanostructure located in the field of monochromatic laser radiation at the fundamental frequency ($\lambda = 1560$ nm) showed that a change in the radiation polarisation direction from parallel to the nanorod to orthogonal leads to a change in the field intensity at the fundamental frequency by a factor of 50. It was also experimentally shown that this change in polarisation increases the emission power at the third-harmonic frequency by a factor of 40 000 [89].

Figure 6 shows a dependence of the third-harmonic generation signal on the excitation radiation polarisation. It can be seen that the third-harmonic generation efficiency is minimum when the excitation radiation is polarised orthogonally to the nanorod ($\varphi = 90°$). A rotation of the polarisation by 90° leads to an increase in the power of the third-harmonic signal by a factor of $4 \times 10^4$. This high sensitivity to polarisation is a consequence of the power (with an exponent of 3) dependence of the third-harmonic generation efficiency on the incident radiation intensity.

Due to the strong polarisation dependence of the third-harmonic generation efficiency in an SHR nanostructure, the latter can be used to design a prototype of an all-optical display, in which SHR nanostructures act as pixels [89]. This optical display is a 4×4 array of SHR nanostructures spaced
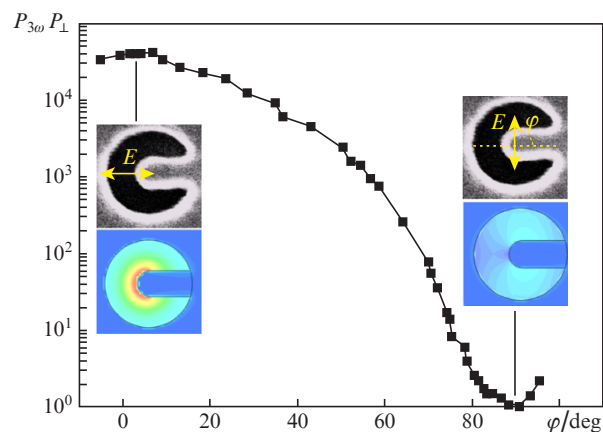


**Figure 6.** (Colour online) Dependence of the third-harmonic generation amplitude on the excitation light polarisation. The insets show the calculated near-field distributions at the fundamental frequency for two different polarisations (shown by yellow arrows).

by a distance of 1 μm (Fig. 7). The display size is determined by the minimum distance between the nanostructures: 500 nm (1/3 excitation wavelength). The nanostructures were formed in a 50-nm-thick aluminium film. The nanorod of each SHR is rotated with respect to the neighbouring nanostructure by an angle of 11.5° (Fig. 7a). The principle of operation of this optical display is as follows. All SHR nanostructures are exposed to femtosecond radiation ($\lambda = 1.56$ μm). If the radiation is polarised along the nanorod of some SHR, only this nanostructure is in exact resonance with the laser field, and this nanostructure becomes an efficient third-harmonic source. Thus, choosing a certain direction of the radiation polarisation vector, one can 'switch on' certain pixels of this display.

Figures 7b and 7c demonstrate the principle of operation of an optical nanodisplay irradiated by a femtosecond laser pulse. A rotation of the polarisation vector leads to a resonance with one of the SHR structures of the display, and this SHR becomes a radiation source at the third-harmonic frequency. For example, to address the first pixel of the display (the square on the left in Fig. 7a), the excitation beam polarisation vector should be directed along the nanorod of the SHR forming this pixel. In this case, an illumination of the display leads to luminescence of only this pixel (Fig. 7b). A rotation of the polarisation vector leads to its coincidence with the direction of the nanorod of another SHR (the square on the right in Fig. 7a). As a result, this pixel is in resonance with the incident radiation, and there is luminescence from only this pixel (Fig. 7c).

Note that ultrafast pixel control can be implemented in an optical display, because the characteristic relaxation time of plasmonic oscillations in aluminium is about 100 as [2].

### 5.2. Nanoprobe of a femtosecond laser pulse

Currently, the measurement of ultrafast (on the femtosecond scale) optical fields with a nanoscale spatial resolution continues to be a hard-to-solve problem. At the same time, these measurements are very important both for understanding the spatiotemporal dynamics of ultrashort pulses [90] and for many scientific and practical applications, e.g., the study of the interaction of light and matter on the nanoscale [91–93].
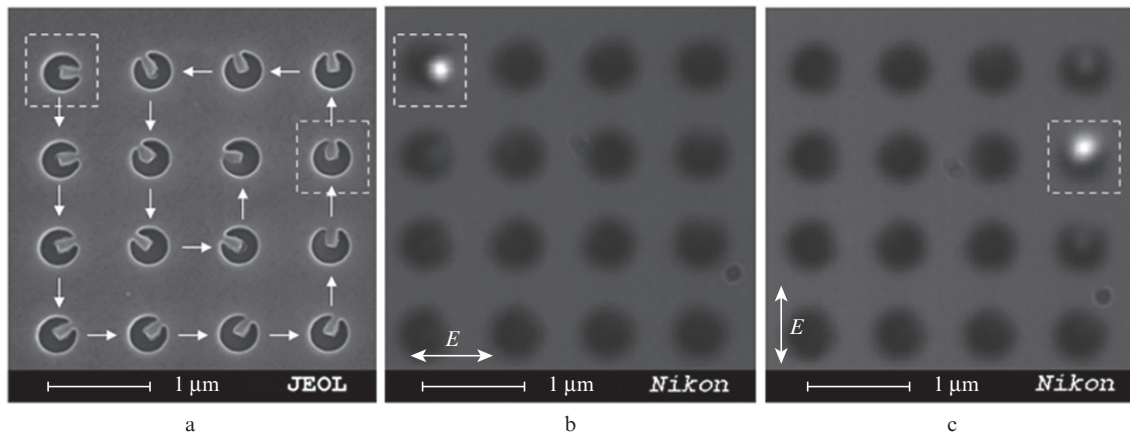
**Figure 7.** All-optical display based on SHR nanostructures fabricated in a 50-nm-thick aluminium film in the form of a 4×4 array with a period of 1 μm: (a) electron microscopy image of the display; (b) display image in an optical microscope, under exposure to light polarised along the nanorod of the first SHR (framed on the left); and (c) display image in an optical microscope, under exposure to light polarised along the nanorod of the SHR framed on the right. The arrows in the SHR nanostructure image (panels b and c) show the polarisation directions of the exciting light.

It is well known that the full knowledge of the parameters of a laser pulse $E(t)$ can be gained by measuring the autocorrelation functions of all orders: $G_n(\tau)$ [90]. Higher order correlation functions can experimentally be found using multi-photon processes. In practice, researchers generally restrict themselves to measurements of the second-order autocorrelation function and subsequent analysis of the results on the assumption that the shape of the laser pulse envelope is *a priori* known. The problem of measuring an ultrashort optical pulse with a nanoscale spatial resolution is even more difficult [94–96].

An SHR nanostructure can be applied as a nanoprobe of a femtosecond laser pulse. When the laser beam intensity is sufficiently high, efficient nonlinear interaction of laser radia-

tion with an SHR nanostructure is implemented. This interaction leads to the generation of harmonics, which can be used to carry out autocorrelation measurements of the duration of the laser pulse exciting the nanostructure. Under these conditions, the optical fields of the second and third harmonics are localised on the nanoscale; therefore, the effective probe size is also on the nanoscale level. Thus, one can measure the temporal properties of femtosecond laser radiation using an SHR.

The SHR structure used as a nanoprobe was fabricated (using a tightly focused ion beam) in a 100-nm aluminium film deposited on an ultrathin (40 nm) membrane [43]. The geometric sizes of the nanostructure were chosen so as to make it possible to implement maximum amplification of the
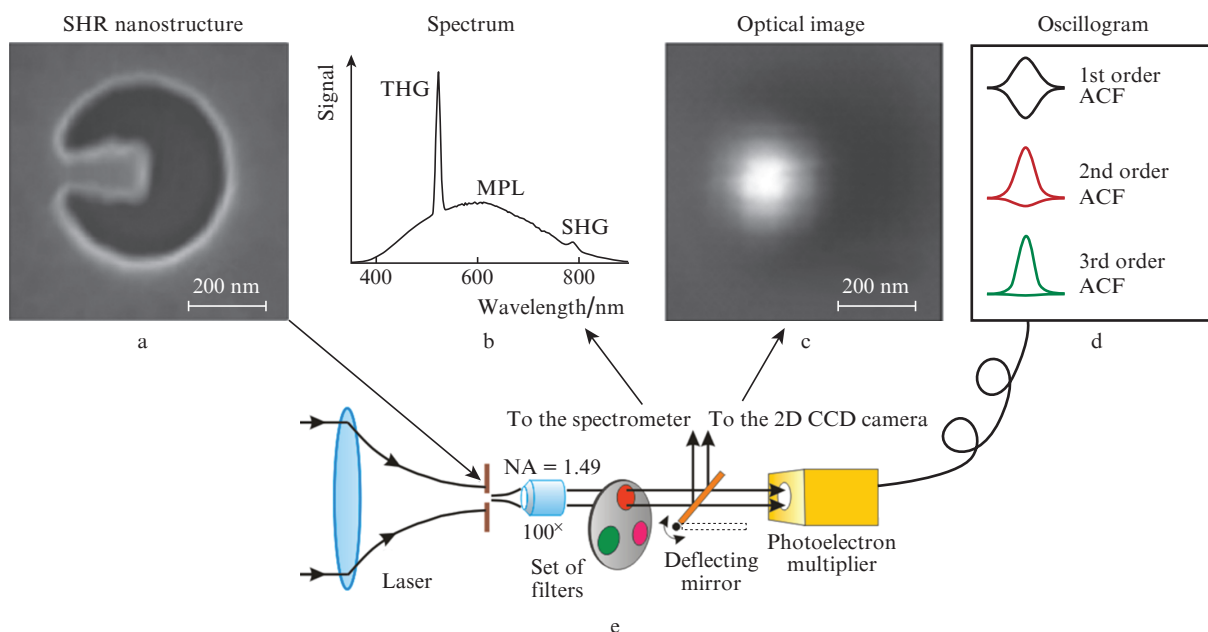


**Figure 8.** SHR nanoprobe of a femtosecond laser pulse: (a) electron microscopy image of the SHR nanostructure; (b) SHR emission spectrum upon excitation by light with $\lambda = 1560$ nm; (c) optical image of the SHR nanostructure at the third-harmonic generation wavelength; (d) autocorrelation functions (ACFs) of the 1st, 2nd, and 3rd orders, measured with the aid of the SHR; and (e) block diagram of the setup for measuring the spatial and temporal properties of femtosecond laser pulses using an SHR nanostructure.

near-field amplitude at the fundamental frequency [43]. The luminescence spectrum of the SHR nanostructure excited by 1560-nm laser radiation contains the second and third harmonics (Fig. 8a). An optical image of the SHR at the third-harmonic wavelength is shown in Fig. 8c.

A schematic of measuring the spatial and temporal properties of femtosecond laser radiation using a single plasmonic SHR nanostructure is shown in Fig. 8. The laser radiation transmitted through a Michelson interferometer entered a microscope and was focused on an SHR nanostructure. The radiation at the fundamental frequency, transmitted through the nanostructure, and the second and third harmonics were collected on a photodetector. The detection of the fundamental, second-, and third-harmonic components made it possible to perform autocorrelation measurements of the first, second, and third orders, respectively. Thus, a nanoprobe based on an SHR nanostructure allows the femtosecond pulse duration to be measured with a nanoscale spatial resolution.

# 6. Conclusions

We have briefly reviewed the results of experimental studies of the linear and nonlinear properties of a single plasmonic SHR nanostructure. The possibilities of efficient generation of harmonics in the IR-to-UV spectral range and multiphoton luminescence from the SHR nanostructure have been shown. A design of SHR-based optical nanodevices has been demonstrated by the example of an all-optical nanodisplay and a nanoprobe for measuring the femtosecond pulse duration.

# References

1. Brongersma M.L., Shalaev V.M. *Science*, **328**, 440 (2010).
2. Stockman M.I., Kling M.F., Kleineberg U., Krausz F. *Nat. Photon.*, **1**, 539 (2007).
3. Balykin V.I., Melentiev P.N. *Usp. Fiz. Nauk* (in press) (2017), DOI: 10.3367/UFNe.2017.06.038163.
4. Kreibig U., Vollmer M. *Optical Properties of Metal Clusters* (Berlin: Springer Verlag, 1995).
5. Bohren C., Huffman D. *Absorption and Scattering of Light by Small Particles* (New York: Wiley, 1998).
6. Liz-Marzaмn L.M. *Langmuir*, **22**, 32 (2006).
7. Klimov V.V. *Nanoplasmonics* (Singapore: Pan Stanford, 2014).
8. Sosa I.O., Noguez C., Barrera R.G. *J. Phys. Chem. B*, **107**, 6269 (2003).
9. Noguez C. *J. Phys. Chem. C*, **111**, 3806 (2007).
10. Khlebtsov B.N., Khlebtsov N.G. *J. Phys. Chem. C*, **111**, 11516 (2007).
11. Melentiev P.N., Afanasiev A.E., Kuzin A.A., Gusev V.M., Kompanets O.N., Esenaliev R.O., Balykin V.I. *Nano Lett.*, **16**, 1138 (2016).
12. Fuchs R., Claro F. *Phys. Rev. B*, **35**, 3722 (1987).
13. Babinet M. *C.R. Acad. Sci.*, **4**, L638 (1837).
14. Jackson J.D. *Classical Electrodynamics* (New York: John Wiley & Sons, 1999).
15. Jain P.K., Huang X., El-Sayed I.H., El-Sayed M.A. *Plasmonics*, **2**, 107 (2007).
16. Garcia M.A. *J. Phys. D: Appl. Phys.*, **44**, 283001 (2011).
17. Sarychev A.K., Shalaev V.M. *Electrodynamics of Metamaterials* (Singapore: World Scientific, 2007).
18. Kumar C.S. (Ed.) *Nanostructured Thin Films and Surfaces* (Weinheim: John Wiley & Sons, 2010) Vol. 5.
19. Lal S., Link S., Halas N.J. *Nature Photon.*, **1**, 641 (2007).
20. Atwater H.A., Polman A. *Nature Mater.*, **9**, 205 (2010).
21. Lee T. *Planar Microwave Engineering* (Cambridge: Cambridge Univ. Press, 2004).
22. Feth N., Linden S., Klein M.W., Decker M., Niesler F.B.P., Zeng Y., Hoyer W., Liu J., Koch S.W., Moloney J.V., Wagener M. *Opt. Lett.*, **33**, 1975 (2008).
23. Rockstuhl C., Zentgraf T., Meyrath T.P., Giessen H., Lederer F. *Opt. Express*, **16**, 2080 (2008).
24. Zentgraf E., Meyrath T.P., Seidel A., Kaiser S., Giessen H., Rockstuhl C., Lederer F. *Phys. Rev. B*, **76**, 033407 (2007).
25. Linden S., Enkrich C., Wegener M., Zhou J., Koschny T., Soukoulis C.M. *Science*, **306**, 1351 (2004).
26. Klein M.W., Enkrich C., Wegener M., Linden S. *Science*, **313**, 502 (2006).
27. Klein M.W., Wegener M., Feth N., Linden S. *Opt. Express*, **15**, 5238 (2007).
28. Klein M.W., Wegener M., Feth N., Linden S. *Opt. Express*, **16**, 8055 (2008).
29. Bethe H.A. *Phys. Rev.*, **66**, 163 (1944).
30. Roberts A. *J. Opt. Soc. Am. A*, **4**, 1970 (1987).
31. García de Abajo F.J. *Opt. Express*, **10**, 1475 (2002).
32. Degiron A., Lezec H.J., Yamamoto N., Ebbesen T.W. *Opt. Commun.*, **239**, 61 (2004).
33. Rindzevicius T., Alaverdyan Y., Sepulveda B., Pakizeh T., Käll M., Hillenbrand R., Aizpurua J., García de Abajo F.J. *J. Phys. Chem. C*, **111**, 1207 (2007).
34. Boyer D., Tamarat P., Maali A., Lounis B., Orrit M. *Science*, **297**, 1160 (2002).
35. Richardson H.H., Hickman Z.N., Govorov A.O., Thomas A.C., Zhang W., Kordesh M.E. *Nano Lett.*, **6**, 783 (2006).
36. Richardson H.H., Carlson M.T., Tandler P.J., Hernandez P., Govorov A.O. *Nano Lett.*, **9**, 1139 (2009).
37. Skirtach A.G., Dejugnat C., Braun D., Susha A.S., Rogach A.L., Parak W.J., Möhwald H., Sukhorukov G.B. *Nano Lett.*, **5**, 1371 (2005).
38. Carslaw H.S., Jaeger J.C. *Conduction of Heat in Solids* (Oxford: Oxford Univ. Press, 1959).
39. Perner M., Feldmann J., Gresillon S., März J., Von Plessen G., Porstendorfer J., Berg K.-J., Berg G. *Phys. Rev. Lett.*, **85**, 792 (2000).
40. Link S., El-Sayed M.A. *Ann. Rev. Phys. Chem.*, **54**, 331 (2003).
41. Khurgin J.B., Sun G. *Phys. Rev. A*, **88**, 053838 (2013).
42. Melentiev P.N., Konstantinova T.V., Afanasiev A.E., Kuzin A.A., Baturin A.S., Balykin V.I. *Laser Phys. Lett.*, **10**, 075901 (2013).
43. Melentiev P.N., Afanasiev A.E., Kuzin A.A., Baturin A.S., Balykin V.I. *Opt. Express*, **21**, 13896 (2013).
44. Pendry J.B., Holden A.J., Robbins D.J., Stewart W.J. *IEEE Trans. Microwave Theory Tech.*, **47**, 2075 (1999).
45. Garcia-Vidal F.J., Martin-Moreno L., Ebbesen T.W., Kuipers L. *Rev. Mod. Phys.*, **82**, 729 (2010).
46. Nezami M.S., Gordon R. *Opt. Express*, **23**, 32006 (2015).
47. Bergman J.G., McFee J.H., Crane G.R. *Appl. Phys. Lett.*, **18**, 203 (1971).
48. Fomichev S., Popruzhenko S., Zaretsky D., Becker W. *Opt. Express*, **11**, 2433 (2003).
49. Melentiev P.N., Afanasiev A.E., Balykin V.I. *Quantum Electron.*, **44**, 547 (2014) [*Kvantovaya Elektron.*, **44**, 547 (2014)].
50. Czaplicki R., Mäkitalo J., Siikanen R., Husu H., Lehtolahti J., Kuittinen M., Kauranen M. *Nano Lett.*, **15**, 530 (2015).
51. Bouhelier A., Beversluis M., Hartschuh A., Novotny L. *Phys. Rev. Lett.*, **90**, 013903 (2003).
52. Lippitz M., van Dijk M.A., Orrit M. *Nano Lett.*, **5**, 799 (2005).
53. Kim S., Jin J., Kim Y.J., Park I.Y., Kim Y., Kim S.W. *Nature*, **453**, 757 (2008).
54. Bar-Elli O., Grinvald E., Meir N., Neeman L., Oron D. *ACS Nano*, **9**, 8064 (2015).
55. Aouani H., Rahmani M., Navarro-Cía M., Maier S. *Nature Nanotech.*, **9**, 290 (2014).
56. Aouani H., Navarro-Cía M., Rahmani M., Maier S.A. *Adv. Opt. Mater.*, **3**, 1059 (2015).
57. Farkas Gy., Toth Cs., Moustaizis S.D., Papadogiannis N.A., Fotakis C. *Phys. Rev. A*, **46**, R3605 (1992).

58. Kim E.M., Elovikov S.S., Murzina T.V., Nikulin A.A., Aktsipetrov O.A., Bader M.A., Marowsky G. *Phys. Rev. Lett.*, **95**, 227402 (2005).

59. Konstantinova T.V., Melentiev P.N., Afanasiev A.E., Kuzin A.A., Starikov P.A., Baturin A.S., Tausenev A.V., Konyashchenko A.V., Balykin V.I. *Quantum Electron.*, **43**, 379 (2013) [*Kvantovaya Elektron.*, **43**, 379 (2013)].

60. Georges A.T. *Phys. Rev. A*, **54**, 2412 (1996).

61. Shalaev V.M. *Nonlinear Optics of Random Media: Fractal Composites and Metal-dielectric Films* (Berlin, Heidelberg: Springer-Verlag, 2000).

62. Fomichev S.V., Zaretsky D.F., Becker W. *Phys. Rev. B*, **79**, 085431 (2009).

63. Petrov G.I., Shcheslavskiy V., Yakovlev V.V., Ozerov I., Chelnokov E., Marine W. *Appl. Phys. Lett.*, **83**, 3993 (2003).

64. Poliakov E.Y., Markel V.A., Shalaev V.M., Botet R. *Phys. Rev. B*, **57**, 14901 (1998).

65. Wang L., Shorokhov A.S., Melentiev P.N., Kruk S., Decker M., Helgert C., Setzpfandt F., Fedyanin A.A., Kivshar Y.S., Neshev D.N. *ACS Photon.*, **3**, 1494 (2016).

66. Hajisalem G., Nezami M.S., Gordon R. *Nano Lett.*, **14**, 6651 (2014).

67. Metzger B., Schumacher T., Hentschel M., Lippitz M., Giessen H. *ACS Photon.*, **1**, 471 (2014).

68. Xu T., Jiao X., Blair S. *Opt. Express*, **17**, 23582 (2009).

69. Reinhold J., Shcherbakov M.R., Chipouline A., Panov V.I., Helgert C., Paul T., Rockstuhl C., Lederer F., Kley E.B., Tünnermann A., Fedyanin A.A. *Phys. Rev. B*, **86**, 115401 (2012).

70. Scalora M., Vincenti M.A., De Ceglia D., Roppo V., Centini M., Akozbek N., Bloemer M.J. *Phys. Rev. A*, **82**, 043828 (2010).

71. Hanke T., Cesar J., Knittel V., Trügler A., Hohenester U., Leitenstorfer A., Bratschitsch R. *Nano Lett.*, **12**, 992 (2012).

72. Hanke T., Krauss G., Träutlein D., Wild B., Bratschitsch R., Leitenstorfer A. *Phys. Rev. Lett.*, **103**, 257404 (2009).

73. Huang L., Cheng J.X. *Ann. Rev. Mater. Res.*, **43**, 213 (2013).

74. Metzger B., Hentschel M., Schumacher T., Lippitz M., Ye X., Murray C.B., Knabe B., Buse K., Giessen H. *Nano Lett.*, **14**, 2867 (2014).

75. Konstantinova T.V., Melentiev P.N., Afanasiev A.E., Kuzin A.A., Starikov P.A., Baturin A.S., Tausenev A.V., Konyashchenko A.V., Balykin V.I. *Zh. Eksp. Teor. Fiz.*, **144**, 27 (2013).

76. Castro-Lopez M., Brinks D., Sapienza R., Van Hults N.F. *Nano Lett.*, **11**, 4674 (2011).

77. Sasanpour P., Rashidian B., Rashidian B., Vossoughi M. *Nano*, **5**, 325 (2010).

78. Melentiev P.N., Kuzin A.A., Afanasiev A.E., Balykin V.I. *Quantum Electron.*, **46**, 414 (2016) [*Kvantovaya Elektron.*, **46**, 414 (2016)].

79. Schwartz O., Oron D. *Nano Lett.*, **9**, 4093 (2012).

80. Mooradian A. *Phys. Rev. Lett.*, **22**, 185 (1969).

81. Dulkeith E., Niedereichholz T., Klar T.A., Feldmann J., von Plessen G., Gittins D.I., Mayya K.S., Caruso F. *Phys. Rev. B*, **70**, 205424 (2004).

82. Melentiev P.N., Konstantinova T.V., Afanasiev A.E., Kuzin A.A., Baturin A.S., Balykin V.I. *Opt. Express*, **20**, 19474 (2012).

83. Ghenuche P., Cherukulappurath S., Taminiau T.H., van Hulst N.F., Quidant R. *Phys. Rev. Lett.*, **101**, 116805 (2008).

84. Bouhelier A., Beversluis M.R., Novotny L. *Appl. Phys. Lett.*, **83**, 5041 (2003).

85. Schuck P., Fromm D.P., Sundaramurthy A., Kino G.S., Moerner W.E. *Phys. Rev. Lett.*, **94**, 017402 (2005).

86. Melentiev P.N., Afanasiev A.E., Kuzin A.A., Zablotskiy A.V., Balykin V.I. *Opt. Express*, **23**, 11444 (2015).

87. Biagioni P., Huang J.S., Hecht B. *Rep. Progr. Phys.*, **75**, 024402 (2012).

88. Shahbazyan T.V. *Nano Lett.*, **13**, 194 (2003).

89. Melentiev P.N., Afanasiev A.E., Kuzin A.A., Baturin A.S., Balykin V.I. *Opt. Lett.*, **38**, 2274 (2013).

90. Sarger L., Oberlé J. *Femtosecond Laser Pulses: Principles and Experiments* (New York: Springer-Verlag, 2005) p. 195.

91. Kubo A., Onda K., Petek H., Sun Z., Jung Y.S., Kim H.K. *Nano Lett.*, **5**, 1123 (2005).

92. Mårsell E., Losquin A., Svärd R., Miranda M., Guo C., Harth A., Lorek E., Mauritsson J., Arnold C.L., Xu H., L'Huillier A. *Nano Lett.*, **15**, 6601 (2015).

93. Jahng J., Brocious J., Fishman D.A., Yampolsky S., Nowak D., Huang F., Apkarian V.A., Wickramasinghe H.K., Potma E.O. *Appl. Phys. Lett.*, **106**, 083113 (2015).

94. Bowlan P., Gabolde P., Trebino R. *Opt. Express*, **15**, 10219 (2007).

95. Extermann J., Bonacina L., Courvoisier F., Kiselev D., Mugnier Y., Dantec R.L., Galez C., Wolf J.P. *Opt. Express*, **16**, 10405 (2008).

96. Li H., Jia Y., Xu Q., Shi K., Wu J., Eklund P.C., Xu Y., Liu Z. *Appl. Phys. Lett.*, **96**, 021103 (2010).